

Phase transitions in interacting domain-wall model

Jae Dong Noh and Doochul Kim

Department of Physics and Center for Theoretical Physics, Seoul National University,

Seoul 151-742, Korea

(December 31, 2021)

Abstract

We investigate the interacting domain-wall model derived from the triangular-lattice antiferromagnetic Ising model with two next-nearest-neighbor interactions. The system has commensurate phases with a domain-wall density $q = 2/3$ as well as that of $q = 0$ when the interaction is repulsive. The $q = 2/3$ commensurate phase is separated from the incommensurate phase through the Kosterlitz-Thouless (KT) transition. The critical interaction strength and the nature of the KT phase transition are studied by the Monte Carlo simulations and numerical transfer-matrix calculations. For strongly attractive interaction, the system undergoes a first-order phase transition from the $q = 0$ commensurate phase to the incommensurate phase with $q \neq 0$. The incommensurate phase is a critical phase which is in the Gaussian model universality class. The effective Gaussian coupling constant is calculated as a function of interaction parameters from the finite-size scaling of the transfer matrix spectra.

I. INTRODUCTION

The triangular-lattice antiferromagnetic Ising model (TAFIM) displays rich critical phenomena. The TAFIM with nearest-neighbor coupling $K < 0$ is described by the Hamiltonian

$$\frac{H}{k_B T} = K \sum_{\langle ij \rangle} s_i s_j \quad (1)$$

where $\langle ij \rangle$ denotes pairs of nearest-neighbor sites of triangular lattice and $s_i = \pm 1$. The ground states of the model are infinitely degenerate due to frustration on each elementary triangle and correspond to a critical state with algebraic decay of correlations [1]. Each ground-state configuration can be mapped to a state of the triangular solid-on-solid (TISOS) model [2] which describes equilibrium shape of a simple-cubic crystal near its $[1;1;1]$ corner or growing of the simple-cubic crystal along the $[1;1;1]$ direction [3], and also of the domain-wall model [1,4]. The latter describes the commensurate-incommensurate (C-IC) phase transitions [5]. When a two-dimensional system with anisotropic interactions has degenerate ground states, excitations from a ground state may take the form of domain walls of striped shapes. A typical example is the axial next-nearest neighbor Ising (ANNNI) model [6]. Though domain-wall type excitations are energetically unfavorable, they also carry a finite amount of entropy. So the system is in an ordered phase without domain-wall excitation (C phase) at low temperatures while it is in a modulated phase with finite density of domain wall for sufficiently high temperatures.

Ground-state properties of the TAFIM are studied by taking the limit $K \rightarrow -\infty$ in Eq. (1) and by assigning statistical weights to each ground-state configuration. The new effective Hamiltonian of interest here can then be written as

$$H = \sum_{\langle ij \rangle} J_{ij} s_i s_j + \sum_{\langle\langle ij \rangle\rangle} J_{ij} s_i s_j + \sum_i h_i s_i : \quad (2)$$

Here, $\langle ij \rangle$ ($\langle\langle ij \rangle\rangle$) denotes pairs of nearest-neighbor (next-nearest-neighbor) sites, J_a (J_{aa}), $a = 1, 2, 3$, are direction-dependent nearest-neighbor (next-nearest-neighbor) couplings and

h is a magnetic field. Each allowed spin configuration $\{s_i\}$ is understood to be one of the ground-state configurations implicitly. The statistical weight for each configuration is proportional to $e^{-H[\{s_i\}]}$.

If there are only nearest-neighbor couplings, the system is equivalent to the non-interacting domain-wall model and can be solved exactly [1,4]. The system exhibits Pokrovsky-Talapov (PT) transition [7] which separates an ordered commensurate (C) phase and a disordered incommensurate (IC) phase. The IC phase is a critical phase which is in the Gaussian model universality class. The free-energy functional of the Gaussian model is given by

$$F = \int d^2r \left[\frac{K_1}{2} \left(\frac{\partial \phi}{\partial x_1} \right)^2 + \frac{K_2}{2} \left(\frac{\partial \phi}{\partial x_2} \right)^2 \right] \quad (3)$$

where K_1 and K_2 are the anisotropic stiffness constants. The Gaussian model has scaling dimensions

$$X_{p,q} = \frac{p^2}{2g} + \frac{q^2}{2} \quad (4)$$

where p and q are integers and $g = 2 \frac{p}{K_1 K_2}$ is called the Gaussian coupling constant [6]. The Gaussian coupling constant is equal to 1/2 throughout the IC phase in this limit [4].

Effect of the magnetic field for the system with $a_x = a_y = 0$ has been studied by numerical transfer-matrix calculations [8] and Monte Carlo simulations [9]. The system undergoes Kosterlitz-Thouless (KT) phase transition [10] from the disordered critical phase to the ordered phase as h increases.

When there are two next-nearest-neighbor couplings ($J_1 \neq 0$; $J_2 \neq 0$; $J_3 = 0$) as well as nearest-neighbor couplings, H in Eq. (2) can be interpreted as a Hamiltonian for an interacting domain-wall system [4]. The nearest-neighbor and next-nearest-neighbor couplings play the role of the fugacity of domain walls and the interaction between domain walls, respectively. There are two types of domain walls and the two next-nearest-neighbor couplings J_1 and J_2 control wall-wall interactions between respective types. In the previous paper [4], we considered the partially interacting domain-wall (PIDW) model where domain walls of

only one type interact with each other ($\epsilon_1 = 0$; $\epsilon_2 \neq 0$ case). The PIDW model is equivalent to the general v -vertex model which in turn is exactly solvable through the Bethe Ansatz method. We obtained exact phase diagram and quantitative understanding of the effect of the interaction in the critical properties of the PIDW model. When the repulsive interaction is strong, the system is in a novel C phase with domain-wall density $q = 1/2$ which is absent in the non-interacting system. In fact, this phase is equivalent to the C phase appearing in the ANNNI model where the interactions between domain walls are assumed to be infinitely repulsive [6]. The IC phase is also the critical phase in the Gaussian model universality class but the Gaussian coupling constant g varies continuously throughout the IC phase.

In this paper, we study the interacting domain-wall (IDW) model where domain walls of both types interact with same strength ($\epsilon_1 = \epsilon_2 \neq 0$ case). We are concerned with the nature of the ordering and the phase transition. We find that the system has an ordered C phase with $q = 2/3$ when the repulsive interaction is sufficiently strong and suggest that the phase transition between the IC phase and the $q = 2/3$ C phase is the KT transition. We argue that the transition is described in the continuum limit by the Gaussian model Eq. (3) with a symmetry-breaking field $V_3 \cos(3\theta(r))$. The repulsive interaction acts as the symmetry-breaking field. When V_3 is sufficiently small, the system is in the critically disordered state with scaling dimensions given in Eq. (4). The Gaussian coupling constant is not constant anymore in the critical region but varies continuously since it is renormalized by the V_3 field. The symmetry-breaking field V_3 has a scaling dimension $X_{3,0}$. As V_3 increases, it becomes relevant in the renormalization group sense. This happens when $X_{3,0} = 2$ (or $g = 9/4$). The phase transition involved in this order-disorder transition is the KT transition. So, we predict that the KT transition occur as the repulsive-interaction strength varies.

On the other side, where the attractive interaction is strong, the domain walls are bounded with each other. We find that, as the chemical potential of domain walls increases, there is a first-order phase transitions from the $q = 0$ C phase to the IC phase accompanied by a finite jump in q .

This paper is organized as follows. In Sec. II we introduce the IDW model and present

the relation between it and the TISO S model. Possible ordered phases in the IDW model are discussed. Unlike the PIDW model, the IDW model is not exactly solvable. So, we investigate the IDW model by numerical diagonalization of the transfer matrix and Monte Carlo simulations. In Sec. III we analyze the eigenvalue spectra of the transfer matrix using the finite-size scaling theory. The transfer matrix applies to a system with a cylinder geometry: infinitely long in one direction, and periodic with a finite size N in the other direction. The calculations are performed for the strip width N up to $N = 18$, corresponding to a transfer matrix of size $2^{18} \times 2^{18}$. Using the finite-size scaling of the eigenvalue spectra, we calculate the Gaussian coupling constant g from which the KT transition point for the repulsive interaction is located. The first-order phase transition line for the attractive interaction is obtained from the eigenvalue spectra and an analytic approximation. In Sec. IV results of Monte Carlo simulations are presented. The simulations are done for a lattice of size up to 120×120 while the domain-wall density is fixed to $2/3$. As well as the specific heat, we also calculate the fluctuations of the position and the density of domain walls since they serve as order parameters for the KT transition. Monte Carlo results are consistent with those of transfer matrix calculations. In Sec. V we summarize our results and discuss the origin of the difference between the PIDW model and the IDW model.

II. THE MODEL AND ITS GROUND STATES

We consider two-dimensional domain-wall model on a finite $N \times M$ triangular lattice with one side of elementary triangle lying along the horizontal direction. The configurations of domain walls are mapped from the ground-state configurations of the TAFIM [4]. The domain walls propagate vertically along the two directions of elementary triangle. We call the domain wall of type 1 (2) if it is left (right) moving. A single chain of domain wall has an entropy $\log 2$ per unit length since there are two ways for domain walls to move. The configurations of domain walls are subject to the restriction that they never be created or annihilated during propagation. Thus, we do not allow the ‘dislocations’ which form

topological excitations. However, effect of such excitations will be discussed briefly in Sec. V.

Domain walls have the chemical potential μ and interaction energy v per unit length. Relationships between $(\mu; v)$ and $(\mu_a; \mu_b)$ of Eq. (2) are derived in Ref. [4]. The interaction energy is assigned to each segment of adjacent-parallel domain walls. The grand-canonical partition function of the IDW model is written as

$$Z_G(x; y) = \sum_{Q=0}^N x^{MQ} \sum_{\{p_1, \dots, p_Q\}} x^{\sum_{i,j} p_{ij}} y^{L(p_1, \dots, p_Q)} \quad (5)$$

where Q is the number of domain walls per row, $x = e^{\mu}$ is the fugacity of a domain wall segment of unit length and $y = e^{-v}$ is the interaction parameter. Here, we use the convention that the 'temperature' of the domain-wall system is absorbed into μ and v . Note that this temperature is different from that of the TAFM. The function $L(p_1, \dots, p_Q)$ counts total length of adjacent-parallel domain walls where $p_i(j)$ denotes the horizontal position of the i -th domain wall at vertical position j . Since configurations with different number of domain walls do not couple with each other at all, the partition sum can be evaluated independently for each Q ;

$$Z_G = \sum_{Q=0}^N x^{MQ} Z_C(y; q)$$

where Z_C is the canonical partition function, representing the second sum in Eq. (5), and $q = Q/N$ is the domain-wall density. The grand-canonical and canonical ensembles are connected through the relation

$$\mu = \frac{1}{MN} \frac{\partial \log Z_G}{\partial q} : \quad (6)$$

Before proceeding the analysis of the IDW model, we digress to explain the equivalence of the domain-wall model and the TISOS model. The TISOS model is a solid-on-solid model on a triangular lattice on which integer-valued heights h_i at site i ($x_i; y_i$) are assigned with the restriction that the height differences between any nearest-neighbor sites are 1 or 2. See Ref. [1] for details. Let n_i be the number of domain walls on the left-hand side of the point $(x_i; y_i)$. Then, the mapping

$$h_i = 3n_i - 2x_i \quad (7)$$

relates a domain-wall configuration to a height configuration. Note that the height variables satisfy the periodic boundary condition $h_{(x_i+N, y_i)} = h_{(x_i, y_i)}$ only if the domain-wall density $q = 2/3$. In this case the TISOS model so constructed, describes the equilibrium shape of a cubic crystal viewed from the $[1;1;1]$ direction. The case of $q \neq 2/3$ corresponds to that viewed from other directions.

'Ground states' of the model for given x and y are the configurations which maximize the Boltzmann weight in Eq. (5). For the attractive interaction ($\epsilon < 0$), a C phase with $q = 0$ (1) is the ground state when $\epsilon < \epsilon^* (\epsilon > \epsilon^*)$. There will be a first-order phase transition along the line $\epsilon = \epsilon^*$ at zero temperature, i.e., $T = 0$. On the other hand, for the repulsive interaction ($\epsilon > 0$), $q = 0$ (1) C phase is the ground state when $\epsilon < 0 (\epsilon > 3\epsilon^*)$. When $0 < \epsilon < 3\epsilon^*$, the $q = 2/3$ C configurations become the ground states. These new ground states correspond to the most densely-packed domain-wall states without interacting pairs and are three-fold degenerate. They are shown in Fig. 1.

To understand finite-temperature behaviors, we should consider excitations from these ground states. Excited states from the $q = 0$ state are formed by domain-wall formations. If the domain walls are far apart from each other (this is the case when the attractive interaction is not so strong), the energy cost is 2ϵ and the wandering entropy gain is $\log 2$ per unit length of domain walls. Thus there will be a phase transition at $\epsilon = -\log 2$.

An excited state of the $q = 1$ state is formed by removing one segment of domain walls from each row. We will call it the domain-wall hole excitation. Unlike a domain wall, the domain-wall hole need not form a continuous path. Thus a single domain-wall hole has a wandering entropy $\log N$ and takes energy cost ϵ per unit length. So the $q = 1$ state is always unstable under domain-wall hole excitations at any value of ϵ .

The $q = 2/3$ C state has complicated excitations. The simplest kind of excitations is generated by locally reversing two units of a domain wall with respect to a vertical axis. Its excitation energy is 2ϵ . This excitation is a local excitation so it cannot destroy the long-range order at low temperatures. Another important excitation is formed by domain boundaries between the three ground-state configurations. This is illustrated in Fig. 2 where

three ground-state configurations of Fig. 1 coexist forming domain boundaries.

Nature of such excitations becomes more transparent when we introduce a coarse-grained field variable as follows. First we assign a height variable h_i to each lattice site according to Eq. (7). The height variables corresponding to the domain wall configuration of Fig. 2 are also shown in Fig. 2 by small numbers. We now group lattice sites into a triangular array of elementary triangles shown as dotted triangles in Fig. 2. To each elementary dotted triangle, we then assign a coarse-grained height variable

$$\tilde{h} = (h_1 + h_2 + h_3)/3 \quad (8)$$

where i 's denote the three sites of the triangle. The values of \tilde{h} for the configuration of Fig. 2 are shown by big numbers in the middle of each dotted triangle. \tilde{h} take integer values and $\tilde{h} = \tilde{h}_0 \pmod{3}$ if local configurations at \mathbf{r} and $\mathbf{r} + \mathbf{a}$ are in the same ground-state configuration. At each boundary, $\tilde{h} = 1$ or 2 . In the continuum limit, the critical behaviors of the system are described by the Gaussian model with free-energy functional F in Eq. (3) if there is no interaction between domain walls. The repulsive interaction favors the coarse-grained height $\tilde{h}(\mathbf{r})$ to be an integer where $\tilde{h}(\mathbf{r})$ denotes \tilde{h} in the continuum limit. So we postulate that the order-disorder phase transition in the IDW model with $q = 2/3$ is described by the Gaussian model with a symmetry-breaking field whose free-energy functional is given by

$$F = \int d^2r \left[\frac{1}{2} K_1 \left(\frac{\partial \tilde{h}}{\partial x_1} \right)^2 + \frac{1}{2} K_2 \left(\frac{\partial \tilde{h}}{\partial x_2} \right)^2 + V_3 \cos(3\tilde{h}(\mathbf{r})) \right] \quad (9)$$

where $\tilde{h}(\mathbf{r}) = \frac{2}{3}\tilde{h}(\mathbf{r})$ and the parameters K_1, K_2 and V_3 are functions of the interaction strength y . It is known that this system has two phases: critically disordered phase (high temperature phase) and the ordered phase (low temperature phase) [10]. In the critical region the model is renormalized to

$$F = \int d^2r \left[\frac{1}{2} \tilde{K}_1 \left(\frac{\partial \tilde{h}}{\partial x_1} \right)^2 + \frac{1}{2} \tilde{K}_2 \left(\frac{\partial \tilde{h}}{\partial x_2} \right)^2 + \tilde{V}_3 \cos(3\tilde{h}(\mathbf{r})) \right] \quad (10)$$

where \tilde{K}_1 and \tilde{K}_2 are renormalized stiffness constants which are functions of K_1, K_2 and V_3 . The scaling dimension of the symmetry-breaking field is $X_{3,0} = 9/(2g)$ with the effective

Gaussian coupling constant $g = 2 \frac{q}{\sqrt{K_1 K_2}}$. In the critical region the symmetry-breaking field is irrelevant (i.e., $X_{3,0} > 2$). The phase transition into the ordered phase occurs at the values of the model parameters which satisfy the relation $X_{3,0} = 2$ and belongs to the universality class of the KT transition. The transition point can be found from the condition $g = 9/4$.

In this section, we presented ground states of the IDW model and the conjecture that the C-IC transition of the IDW model with the repulsive interaction at $q = 2/3$ is described by the free-energy functional given in Eq. (9). In the next two sections, we will confirm our conjecture by transfer matrix calculations and Monte Carlo simulations.

III. FINITE-SIZE SCALING ANALYSIS OF TRANSFER-MATRIX SPECTRA

We study the IDW model on a finite lattice with width N and height M using the transfer matrix. The grand-canonical partition function Z_G in Eq. (5) is written as

$$Z_G = \sum_{Q=0}^N x^{M-Q} \text{Tr} T_Q^M$$

where T_Q is a transfer matrix which acts on the $N C_Q$ dimensional space spanned by statekets $|n_1; \dots; n_Q\rangle$ specifying positions of Q domain walls. The matrix element $\langle n_1^0; \dots; n_Q^0 | T_Q | n_1; \dots; n_Q \rangle$ represents the Boltzmann weight for a domain-wall configuration between two rows of a lattice as shown in Fig. 3.

We denote the p -th largest eigenvalue of T_Q by $e^{E_Q^p}$ and E_Q^p will be called the energy of the p -th excited level. In the limit $M \rightarrow \infty$, the canonical partition function is given by the largest eigenvalue, i.e., $Z_C = e^{M E_Q^0}$. In the IC phase, $q = Q/N$ varies continuously as a function of β and μ . When q is given, the chemical potential should be chosen so as to satisfy the finite-size version of Eq. (6)

$$= \frac{E_{Q+1}^0 - E_{Q-1}^0}{2N} :$$

The eigenvalue spectrum for a conformally invariant system follows the universal scaling form

$$\text{Re } E(N) = N f_1 + \frac{2}{N} X \frac{c}{12} + o\left(\frac{1}{N}\right) \quad (11)$$

where c is the central charge, X is the scaling dimension of the operator associated with eigenstate ψ , γ is an anisotropy factor, and f_1 is the bulk free energy per site [11]. The IC phase of the domain-wall system is the critical phase in the universality class of the Gaussian model whose central charge is 1 and scaling dimensions are given in Eq. (4). In the previous paper [4], we showed that the p -th excited level of T_Q leads to the scaling dimension $X_{p,0}$ and excitations of the largest eigenvalues of T_{Q-Q} relative to that of T_Q lead to $X_{0,q}$. Using this knowledge, we can estimate the Gaussian coupling constant by an estimator $g(N)$ defined by

$$g(N) = \lim_{N \rightarrow \infty} \frac{\text{Re}(E_{Q+1}^0 + E_{Q-1}^0 - 2E_Q^0)}{2\text{Re}(E_Q^1 - E_Q^0)}$$

which should approach g as $N \rightarrow \infty$. A sequence of $g(N)$ is obtained by numerical diagonalization of transfer matrix for a system of width N up to 18. We present the estimates in Fig. 4 (a) and Fig. 4 (b) for the repulsive ($\gamma < 1$) and attractive ($\gamma > 1$) case, respectively for several values of γ . The curve for $\gamma = 0.2$ in Fig. 4 (a) is noticeable. $g(N)$ apparently does not converge to a finite value as N increases when $q = 2=3$. It means that when $\gamma = 0.2$ the eigenvalue spectrum does not follow the finite-size scaling form of Eq. (11) and that the system is no longer in a critical phase. We gave an argument in the previous section that the system undergoes a phase transition into the ordered phase as the repulsive interaction becomes strong and that the Gaussian coupling constant should be $g=4$ at the transition point. Thus we estimate the critical interaction strength y_c by solving the equation $g(N) = g=4$ numerically. For this purpose, we find that the alternative estimators defined by

$$g(N) = \frac{6E_Q^0(N+3) - E_Q^0(N)}{E_Q^1(N+3) - E_Q^0(N+3) - E_Q^1(N) + E_Q^0(N)}$$

converge better. The solutions of $g(N) = g=4$, denoted by $y_1(N)$, are given in Table I. The strip-width dependence of $y_1(N)$ follows from corrections to scaling of the eigenvalues. At the KT transition point there are logarithmic corrections due to the presence of a marginally irrelevant field [9]. Thus the sequence of estimator $y_1(N)$ is extrapolated by fitting it to the

form $y_1(N) = y_2 + a/(b + \log N)$. Since the sequence y_2 thus obtained also show slow convergence, we fit it again to the same form and obtain the result $y_c = 0.252 \pm 0.003$. See Table I.

When $y < y_c$, there appears the $q = 2/3$ C phase. As in the $q = 1/2$ C phase of the PDW model, q remains locked to the value $2/3$ in the range $y_c < y < y_{c2}$. Estimates of the chemical potential at the lower and upper boundaries of the C phase are given by

$$\epsilon(N) = \epsilon_{Q_0-1}^0(N) - \epsilon_{Q_0}^0(N)$$

where $Q_0 = 2N/3$. Since they are evaluated from finite-size systems, we should know the finite-size scaling form of $\epsilon(N)$. Due to the marginal corrections at the phase boundary, the largest eigenvalues for $Q = Q_0 - m$ is expected to have scaling forms

$$\epsilon_{Q_0-m}^0 = \epsilon_{Q_0}^0 - m + \frac{g}{N} m^2 + O\left(\frac{1}{N \log N}\right) :$$

It then follows that $\epsilon(N)$ behaves as

$$\epsilon(N) = -\frac{g}{N} + O\left(\frac{1}{N \log N}\right) :$$

Accordingly, we estimate y_c by fitting $\epsilon(N)$ to the equation $\epsilon(N) = -a/N + b/N \log N$. The result is shown in Fig 5.

We have thus determined the phase boundary of the $q = 2/3$ phase using the finite-size scaling of the eigenvalue spectra of the transfer matrix. Next, we consider the system near the $q = 0$ C phase. As the chemical potential increases, domain walls begin to form. They form a free or bound state depending on the interaction strength y . To see this, we calculate in the Appendix the ground-state energy and un-normalized eigenket of T_Q for $Q = 2$ from the Bethe Ansatz method. The results for the maximum eigenvalue and the eigenket are

$$\begin{aligned} E_2^0 &= -2 \log 2; & |j\rangle &= \prod_{m < n}^P |j_m; n_i\rangle & \text{if } y < \frac{3}{2} \\ E_2^0 &= -\log 2y + \frac{1}{2(y-1)}; & |j\rangle &= \prod_{m < n}^P (2(y-1))^{(n-m)} |j_m; n_i\rangle & \text{if } y > \frac{3}{2}; \end{aligned} \quad (12)$$

where the thermodynamic limit is taken. The eigenket has a qualitatively different properties on both side of $y = 3/2$ line.

As can be seen from Eq. (12), domain walls form a free state when $y = 3=2$. So, the C-IC transition is the PT transition as in the non-interacting and the PIDW models. The domain wall density has a square-root dependence on the chemical potential

$$q = (\mu_c)^{1/2}$$

with the critical chemical potential $\mu_c = \log 2$.

When $y = 3=2$, Eq. (12) shows that domain walls form a bounded state. The two domain walls are bounded with the mean distance

$$d_0 = \lim_{n \rightarrow \infty} \frac{4(y-1)^2}{4(y-1)^2 - 1} :$$

The ground-state energy of the bounded state consists of two parts $E_2^0 = E_{cm} + E_{int}$; where $E_{cm} = \log 2$ comes from free motions of the center of mass of the two domain walls and $E_{int} = \log(y+1) - 4(y-1)$ from the effective interaction. To generalize Eq. (12) for $Q = 3$ where exact results are not available, we construct a simple approximation for E_Q^0 as a sum of E_{cm} and E_{int} . Thus we write the ground-state energy of the T_Q for $Q \neq 2$ as

$$\begin{aligned} E_Q^0 &= E_{cm} + (Q-1)E_{int} \\ &= \log 2 + (Q-1) \log y + \frac{1}{4(y-1)} \end{aligned} \quad (13)$$

This approximation will be called the two-domain-wall approximation. It should be valid as long as $q \ll 1=d_0$. When $q > 1=d_0$, domain walls feel additional statistical repulsive interactions. This statistical repulsions then drive the system into the IC phase. Within the two-domain-wall approximation, the domain-wall system undergoes a first order C-IC transition from the $q = 0$ C phase to the IC phase. Since Eq. (13) is linear in Q , the transition occurs at the chemical potential

$$\mu_0 = \log y + \frac{1}{4(y-1)} \quad (14)$$

while q_0 , the discontinuity of q at the transition, can be taken to be $1=d_0$ approximately.

μ_0 and q_0 are also determined numerically. When $y = 3=2$, E_Q^0 for finite N obtained from numerical diagonalization of T_Q becomes concave downward in some region $0 < Q < Q_0$

indicating a first order phase transition. We took the convex envelop of E_Q^0 and estimated q_0 and q_0 from the slope of the straight line enveloping the concave region and from the point where the straight line and the curve of E_Q^0 are tangential, respectively. The results are shown in Figs. 6 for five values of N . These are compared with Eq. (14) and the approximation $q_0 = 1/d_0$ in Figs. 6.

Resulting phase diagram of the IDW model as obtained from the transfer-matrix calculations is summarized in Fig. 7. This is the main result of this work.

IV. RESULTS OF MONTE CARLO SIMULATIONS

In the previous section, the assumption that the repulsive interaction induces the KT transition at the $q = 2/3$ C phase boundary is used to estimate the critical interaction strength y_c from the numerical diagonalization of the transfer matrix. In this section, we will confirm the nature of the phase transition more directly by Monte Carlo simulations at $q = 2/3$ on a finite $L \times L$ lattice.

At the KT transition point, there is no diverging peak in the specific heat. So, we should study another quantities such as the renormalized stiffness constants \tilde{K}_1 and \tilde{K}_2 in Eq. (10). They can be evaluated from the linear response

$$\frac{\partial \langle \phi \rangle}{\partial x_k} = \frac{v_k}{\tilde{K}_k}$$

produced by an additional free energy term

$$F_k = -v_k \int d^2r \frac{\partial \phi}{\partial x_k}$$

where $k = 1$ or 2 . From the fluctuation-dissipation theorem, we see that

$$\begin{aligned} \frac{1}{\tilde{K}_k} &= \lim_{v_k \rightarrow 0} \frac{1}{v_k} \frac{\partial \langle \phi \rangle}{\partial x_k} \\ &= \frac{1}{V} \int d^2r \int d^2r^0 \frac{\partial \langle \phi(r) \rangle}{\partial x_k} \frac{\partial \langle \phi(r^0) \rangle}{\partial x_k} = \frac{1}{V} \int d^2r \int d^2r^0 \frac{\partial \langle \phi(r) \rangle}{\partial x_k} \frac{\partial \langle \phi(r^0) \rangle}{\partial x_k} \end{aligned}$$

where V is the volume and \bar{h}_0 denotes the average with $v_k = 0$. These quantities are called helicity moduli and serve as order parameters for systems exhibiting the KT transition, e.g., XY model [12].

Using Eqs. (7) and (8) which connect the Gaussian model and the domain-wall model, $\bar{\kappa}_k$ can be written in terms of the quantities of the domain-wall model as

$$\frac{1}{\bar{\kappa}_k} = \frac{4}{L^2} \sum_{i,j} x_{i,j}^2 \left(\sum_k n_i \frac{2}{3} \delta_{k,1} - \sum_k n_j \frac{2}{3} \delta_{k,1} \right) = \sum_k \left(\sum_i n_i \frac{2}{3} \delta_{k,1} - \sum_j n_j \frac{2}{3} \delta_{k,1} \right)$$

where $\sum_k n_i \frac{2}{3} \delta_{k,1} = \sum_k n_i \frac{2}{3} \delta_{k,1}$ is the unit vector along the k direction and $\delta_{k,1}$ is the Kronecker delta function. From the definition of n_i , we see that

$$\begin{aligned} n_i &= \begin{cases} 1 & \text{; if there is a domain wall between } (x_i, y_i) \text{ and } (x_i, y_i) + e_1 \\ 0 & \text{; otherwise} \end{cases} \\ n_i &= \begin{cases} 1 & \text{; if there is a domain wall of type 1 between } (x_i, y_i) \text{ and } (x_i, y_i) + e_2 \\ 1 & \text{; if there is a domain wall of type 2 between } (x_i, y_i) \text{ and } (x_i, y_i) + e_2 \\ 0 & \text{; otherwise} \end{cases} \end{aligned}$$

Using this relation, we can write the expression for the stiffness constants as

$$\begin{aligned} \frac{1}{\bar{\kappa}_1} &= \frac{4}{L^2} \sum_i h_i^2 - \sum_i h_i^2 \\ \frac{1}{\bar{\kappa}_2} &= \frac{4}{L^2} \sum_i \frac{Q_2 - Q_1}{2} = \frac{4}{L^2} \sum_i x_i^2 - \sum_i x_i^2 \end{aligned} \quad (15)$$

where Q ($Q_{1,2}$) is the total length of the domain walls (of type 1 or 2) and $x_i = p_i(L) - p_i(0)$ is the difference of the position of the i -th domain wall at the top to that at the bottom. The equations show that $\bar{\kappa}_1$ controls the fluctuations of the domain-wall length and $\bar{\kappa}_2$ the fluctuations of the domain-wall positions.

We performed simulations with the periodic boundary condition along the horizontal direction and the free boundary condition along the vertical direction with domain-wall density fixed to $2/3$. Updating rule from a domain-wall configuration $\{p_i(j)\}_j$ to $\{p_i^0(j)\}_j$ is

as follows. There are four kinds of configurations for any (i, j) ;

- (i) $p_i(j-1) + 1/2 = p_i(j) = p_i(j+1) - 1/2$
- (ii) $p_i(j-1) - 1/2 = p_i(j) = p_i(j+1) + 1/2$
- (iii) $p_i(j-1) - 1/2 = p_i(j) = p_i(j+1) - 1/2$
- (iv) $p_i(j-1) + 1/2 = p_i(j) = p_i(j+1) + 1/2$:

A given configuration can be changed locally only for the cases (iii) and (iv). For the case (iii), $p_i(j)$ is updated to $p_i^0(j) = p_i(j) + 1$ with a probability $y^{L(fpg) - L(fpg)}$ provided $p_{i+1}(j) \leq p_i(j) - 1$, while for the case (iv), $p_i(j)$ is updated to $p_i^0(j) = p_i(j) - 1$ with a probability $y^{L(fpg) - L(fpg)}$ provided $p_{i-1}(j) \leq p_i(j) - 1$. For other cases, the configuration is not altered. Noting that the updating trial at (i, j) has nothing to do with domain walls $(i-2, j-2)$, we divide the set $f(i, j)$ into four parts depending on whether i, j are even or odd and choose randomly one of the four subsets and update the whole domain walls in that subset.

The free boundary condition along the vertical direction is necessary to calculate the quantities $\sum_i p_i X_i$. On the other hand, one should adopt, in principle, a grand canonical ensemble in which the domain-wall number could vary in order to calculate the fluctuations of the domain-wall number. But it poses too much technical difficulty, so we measure instead fluctuations of the domain-wall number in a fixed rectangular region of size $(L=2) \times L$ during simulations of the $L \times L$ system. For such an ensemble, an elementary probability consideration shows that χ_1^2 should be given by

$$\frac{1}{\chi_1^2} = \frac{16}{L^2} \langle Q^2 \rangle - \langle Q \rangle^2$$

where Q is the number of domain walls inside the $(L=2) \times L$ region.

In Fig. 8, we present results for the energy fluctuations C which is defined by

$$C = \frac{1}{L^2} \langle [L(fpg) - hL(fpg)]^2 \rangle$$

for systems of linear size $L = 12, 36, 60, 90$ and 120 . As expected, there is a converging peak instead of a diverging peak. The peak position is below the estimated critical interaction

strength, i.e., at the low-temperature region. This is consistent with the behaviors in the XY model where the peak is at the high-temperature region. The KT transition in the XY model is the vortex-antivortex unbinding transition and that in the IDW model is a spontaneous symmetry-breaking transition. The effects of the vortex-antivortex and the symmetry-breaking field have a dual relation [10]

$$Z(2/K; y_0; y_p) = Z(p^2=2/K; y_p; y_0) (p=2/K)^N$$

where K is the inverse temperature, y_0 is the fugacity of the vortex and antivortex, and y_p is the strength of the symmetry-breaking field. We see that the high and low temperature regions are inverted.

Figs. 9(a) and (b) show the measured values of $1/\bar{\kappa}_1$ and $1/\bar{\kappa}_2$, respectively, as a function of y for several values of L . Though we did not try to extract the quantitative results, they show manifest crossover behaviors near $y = y_c$. They become smaller and smaller in the ordered regions as the system size L increases and the points at which the crossover behaviors set in become closer and closer to the estimated critical-interaction strength y_c . These behaviors are in accord with Monte Carlo results of the XY model [12]. Finally, Fig. 9(c) shows the values of g obtained from the relation $g = 2 \sqrt{\bar{\kappa}_1 \bar{\kappa}_2}$. The coupling constant estimated in this way is in good agreement with that obtained from the transfer matrix spectra. That the values of g at y_c fall short of the expected value $g=4$ is attributed to slow convergence arising from the presence of logarithmic corrections. From these numerical results, we conclude that the phase transition belongs to the universality class of the KT transition.

V. SUMMARY AND DISCUSSION

In summary, we have investigated the phase transitions in the IDW model. There are three phases: the $q = 0$ and $q = 2=3$ C phases and the IC phase. The transition between the $q = 0$ C phase and the IC phase is the PT transition when the interactions between

domain walls are repulsive or weakly attractive. When the interaction is strongly attractive, it becomes the first-order phase transition with a discontinuity of the domain-wall density. The nature of the transitions are altered because of formation of bounded domain-wall states. As to the transition between the $q = 2/3$ C phase and the IC phase, we suggested the free-energy functional is that of the Gaussian model with a symmetry-breaking field with the scaling dimension $X_{3,0}$. The symmetry-breaking field accounts for effects of the repulsive interaction and induces the KT transition from the critical phase to the ordered phase. We confirmed this scenario by calculating the stiffness constants from the Monte Carlo simulations. From the transfer matrix method, we calculated the Gaussian coupling constant in the IC phase and the critical interaction strength. Phase boundaries in the T - μ plane are also determined from the transfer matrix method.

The domain-wall model is constructed from the TAFIM with the restriction that three spins on elementary triangles cannot have the same sign. If this is allowed the excitation of this type constitutes a topological excitation where two-domain walls are created or annihilated [4]. It plays the role of vortex and antivortex excitation in the XY model. The scaling dimension of the excitation is $X_{0,2}$. Since it is irrelevant when $g > 1$, it cannot alter the nature of the C-IC transition of the $q = 2/3$ C phase where $g = 9/4$ [13].

In the PIDW model where the interaction and the chemical potential is anisotropic the repulsive interaction stabilizes the $q = 1/2$ C phase. But, the phase transition is of the PT type. Thus the anisotropy plays an important role in determining the nature of the phase transition. The anisotropy produces an extra term in the free-energy functional which couples to the differences of the number of domain walls of type 1 and 2. So the PIDW model would be described by the effective free-energy functional

$$F = \int d^2r \left[\frac{1}{2} K_1 \left(\frac{\partial \phi}{\partial x_1} \right)^2 + \frac{1}{2} K_2 \left(\frac{\partial \phi}{\partial x_2} \right)^2 + V_p \cos(\phi(x)) \right] \quad (5)$$

where the symmetry-breaking field accounts for the ordering induced from domain-wall interactions and the linear term $\partial \phi / \partial x_2$ accounts for the effect of the anisotropy. In this model, the phase transition is induced by the coupling V_p . It induces a domain-wall type

excitation and the phase transition is in the universality class of the PT transition [5].

Even though we studied only the equilibrium properties of the IDW model in this work, non-equilibrium version is also of interest since it describes a driven domain-wall model or the hypercube stacking model [3] and also the charge conduction in the charge-density-wave system [14]. We leave it for further study.

ACKNOWLEDGMENTS

This work is supported by Korea Science and Engineering Foundation through the Center for Theoretical Physics, and also by Ministry of Education through Basic Science Research Institute, of Seoul National University.

APPENDIX A :

In this appendix, we derive expressions for the largest eigenvalue and the corresponding eigenket $|j\rangle$ of the transfer matrix T_Q for $Q = 2$ analytically. The eigenket is of the form

$$|j\rangle = \sum_{1 \leq m < n \leq N} a(m; n) |j\rangle_{m; n}$$

where $|j\rangle_{m; n}$ denotes a state with two domain walls at sites m and n . The eigenvalue equation $T_2 |j\rangle = \lambda |j\rangle$ gives linear equations for coefficients $a(m; n)$:

$$a(m; n) = \sum_{m^0 < n^0} a(m^0; n^0) \langle m; n | T_2 |j\rangle_{m^0; n^0} \quad : \quad (\text{A } 1)$$

When T_2 is applied to a stateket $|j\rangle_{m; n}$, it generates a new stateket:

$$T_2 |j\rangle_{m; n} = \begin{cases} |j\rangle_{m; n} + |j\rangle_{m+1; n} + |j\rangle_{m+1; n+1} + |j\rangle_{m+1; n+1} & \text{if } n > m+1 \\ y |j\rangle_{m; n} + |j\rangle_{m+1; n} + y |j\rangle_{m+1; n+1} & \text{if } n = m+1 \end{cases}$$

where y is the interaction parameter. Thus Eq. (A 1) becomes

$$a(m; n \neq m+1) = a(m; n) + a(m-1; n-1) + a(m; n-1) + a(m-1; n) \quad (\text{A } 2)$$

$$a(m; n = m+1) = y a(m; m+1) + y a(m-1; m) + a(m-1; m+1) \quad : \quad (\text{A } 3)$$

These equations are solved by the Bethe Ansatz

$$a(m; n) = A_{12} z_1^m z_2^n + A_{21} z_1^n z_2^m \quad (\text{A } 4)$$

where A_{12}, A_{21}, z_1 and z_2 are constants to be found. Eq. (A 2) is automatically satisfied by $a(m; n)$ given in Eq. (A 4) provided the eigenvalue is

$$\lambda = (1 + z_1)(1 + z_2) \quad :$$

We can make Eq. (A 3) be satisfied by imposing the condition that

$$\begin{aligned} & [a(m; n) + a(m-1; n-1) + a(m; n-1) + a(m-1; n)]_{n=m+1} \\ & = y a(m; m+1) + y a(m-1; m) + a(m-1; m+1) \quad : \end{aligned}$$

This gives the relation between A_{12} and A_{21} as

$$\frac{A_{12}}{A_{21}} = \frac{1 - (y - 1) \frac{1}{z_1} + z_2}{1 - (y - 1) z_1 + \frac{1}{z_2}} :$$

If we use a periodic boundary condition $a(n; m + N) = a(m; n)$, we obtain the equations for z_1 and z_2 :

$$z_1^N = \frac{A_{21}}{A_{12}}; \quad z_2^N = \frac{A_{12}}{A_{21}} :$$

Multiplying the two equations together gives $(z_1 z_2)^N = 1$ which implies that $z_1 z_2 =$ where is an N -th root of unity. The eigenvector corresponding to the maximum eigenvalue comes from the solution with $= 1$ which means that $z_1 = 1 = z_2 = z$. The value of z is determined from the equation

$$z^N = \frac{1 - 2(y - 1)z}{1 - \frac{2(y - 1)}{z}} : \quad (A 5)$$

The solutions of Eq. (A 5) is given by

$$z = \begin{cases} \approx 2(y - 1) + O\left(\frac{1}{(2y - 2)^N}\right) & \text{if } y > \frac{3}{2} \\ \approx 1 + O\left(\frac{1}{N}\right) & \text{if } y = \frac{3}{2} \end{cases} :$$

In the limit $N \rightarrow \infty$, this gives the eigenvalues and eigenvectors presented in Eq. (12).

Unfortunately the Bethe Ansatz works only for $Q = 2$ and fails when $Q = 3$. Thus we are not able to get analytic results for general Q . However, the solution for $Q = 2$ provides a useful approximation near the $q = 0$ C to IC transition as discussed in Sec. III.

REFERENCES

- [1] H. W. J. Blöte and H. J. Hilhorst, J. Phys. A : Math. Gen. 15, L631 (1982).
- [2] B. Nienhuis, H. J. Hilhorst and H. W. J. Blöte, J. Phys. A : Math. Gen. 17 3559, (1984).
- [3] B. M. Forrest and L. H. Tang, Phys. Rev. Lett. 64, 1405 (1990).
- [4] J. D. Noh and D. Kim, Phys. Rev. E 49, 1943 (1994).
- [5] P. Bak, Rep. Prog. Phys. 45, 587 (1982).
- [6] J. Villian and P. Bak, J. Phys. (Paris) 42, 657 (1991).
- [7] V. L. Pokrovsky and A. L. Talapov, Phys. Rev. Lett. 42, 65 (1979).
- [8] H. W. J. Blöte, M. P. Nightingale, X. N. Wu and A. Hoogland, Phys. Rev. B 43, 8751 (1991).
- [9] H. W. J. Blöte and M. P. Nightingale, Phys. Rev. B 47, 15046 (1993).
- [10] J. M. Kosterlitz and D. J. Thouless, J. Phys. C 6, 1181 (1973); J. M. Kosterlitz, J. Phys. C 7, 1046 (1974); J. V. Jose, L. P. Kadano, S. Kirkpatrick and D. R. Nelson, Phys. Rev. B 16, 1217 (1977).
- [11] J. L. Cardy, Phase transitions and critical phenomena vol. 11, edited by C. Domb and J. L. Lebowitz (Academic Press, 1987); D. Kim and P. A. Pearce, J. Phys. A 20, L451 (1987).
- [12] C. Ebner and D. Stroud, Phys. Rev. B 28, 5053 (1983); W. Y. Shih, C. Ebner and D. Stroud, Phys. Rev. B 30, 134 (1984); H. Weber and P. Minnhagen, Phys. Rev. B 37, 5986 (1988).
- [13] D. P. Landau, Phys. Rev. B 27, 5604 (1983).
- [14] G. G nner, Rev. Mod. Phys. 60, 1129 (1988).

Table Caption

Table I. The transfer-matrix calculation of the KT transition point of the IDW model. Estimates of the critical interaction strength $y_1(N)$ is found by solving the equation $g(N) = 9/4$ by the Newton iteration method. The sequence of $y_1(N)$ is fitted to the form $y_1(N) = y_2 + a/(b + \log N)$ to obtain a sequence of extrapolated values $y_2(N)$. y_c is estimated by fitting $y_2(N)$ again to the same asymptotic form. The error is estimated from the difference between y_c and $y_2(9)$

Figure Captions

Fig. 1. Three ground states of the domain-wall system with repulsive interactions when $0 < \gamma < 3$. The broken line represents a triangular lattice and solid line represents sections of the domain wall. Each ground state is obtained by periodic repetitions of each unit in the vertical direction.

Fig. 2. An excited state of the domain-wall system with repulsive interactions. The small numbers on vertices of a triangular lattice denote heights h_i of an equivalent TISOS configuration and the large numbers in dotted triangles denote the coarse-grained heights \tilde{h} .

Fig. 3. An example of a domain-wall configuration in successive two rows of a triangular lattice of width $N = 6$. The domain-wall configuration of the lower row is represented by the stateket $|1;2;3;5\rangle$ while that of the upper one is represented by $|1;3;4;5\rangle$. The transfer-matrix element $\langle 1;3;4;5 | T_{Q=4} | 1;2;3;5 \rangle$ denotes the Boltzmann weight of the above configuration and is equal to y .

Fig. 4 (a). Estimates of the Gaussian coupling constant $g(N)$ as a function of q for several values of y . The symbols $\square, \triangle, +, \times$, and \circ correspond to $N = 6, 9, 12, 15$, and 18 , respectively. The values of y are $0.2, 0.4, 0.6, 0.8$, and 1.0 from top to bottom at each values of q . The broken line denotes the line $g = 9/4$. (b) Same as in (a) but for the values of y $1.0, 1.1, 1.2, 1.3, 1.4$, and 1.5 from top to bottom.

Fig. 5. Phase boundary of the $q = 2/3$ C-IC transition in the γ - y plane. γ_c are obtained by extrapolating $\gamma_c(N)$. The broken line is drawn at the critical interaction strength $y = 0.252$. γ_c^+ and γ_c^- merge into a single value near that line. Solid lines are guides to the eye.

Fig. 6. Estimates of d_0 (a) and q_0 (b) obtained from transfer-matrix calculations (symbols). The two-domain-wall approximation for d_0 and the approximation $q_0 = 1/d_0$ are also shown in (a) and (b), respectively, by solid lines.

Fig. 7. Phase diagrams of the IDW model with the repulsive ($\gamma > 0$) and attractive ($\gamma < 0$) interactions. The solid lines ($\gamma > 0$) denote the PT transition, the broken line ($\gamma < 0$) the KT transition and the dotted line ($\gamma = 0$) the first-order transition. The PT transition lines are

straight lines with slope $-1 = \log 2$.

Fig. 8. Monte Carlo results for the energy fluctuation C . This result indicates that the energy fluctuation remains finite when the system enters the ordered phase. The broken line is drawn at $y = 0.252$.

Fig. 9. Monte Carlo results for the renormalized stiffness constants \bar{K}_1 (a), \bar{K}_2 (b) and the Gaussian coupling constant g (c). They show characteristic behaviors of the KT transition.

TABLES

N	Y_1	Y_2	Y_c
3	0.170790486223	0.265782	0.252
6	0.197135051080	0.256660	
9	0.206717177287	0.255360	
12	0.211836668182		
15	0.215121556318		

Table I

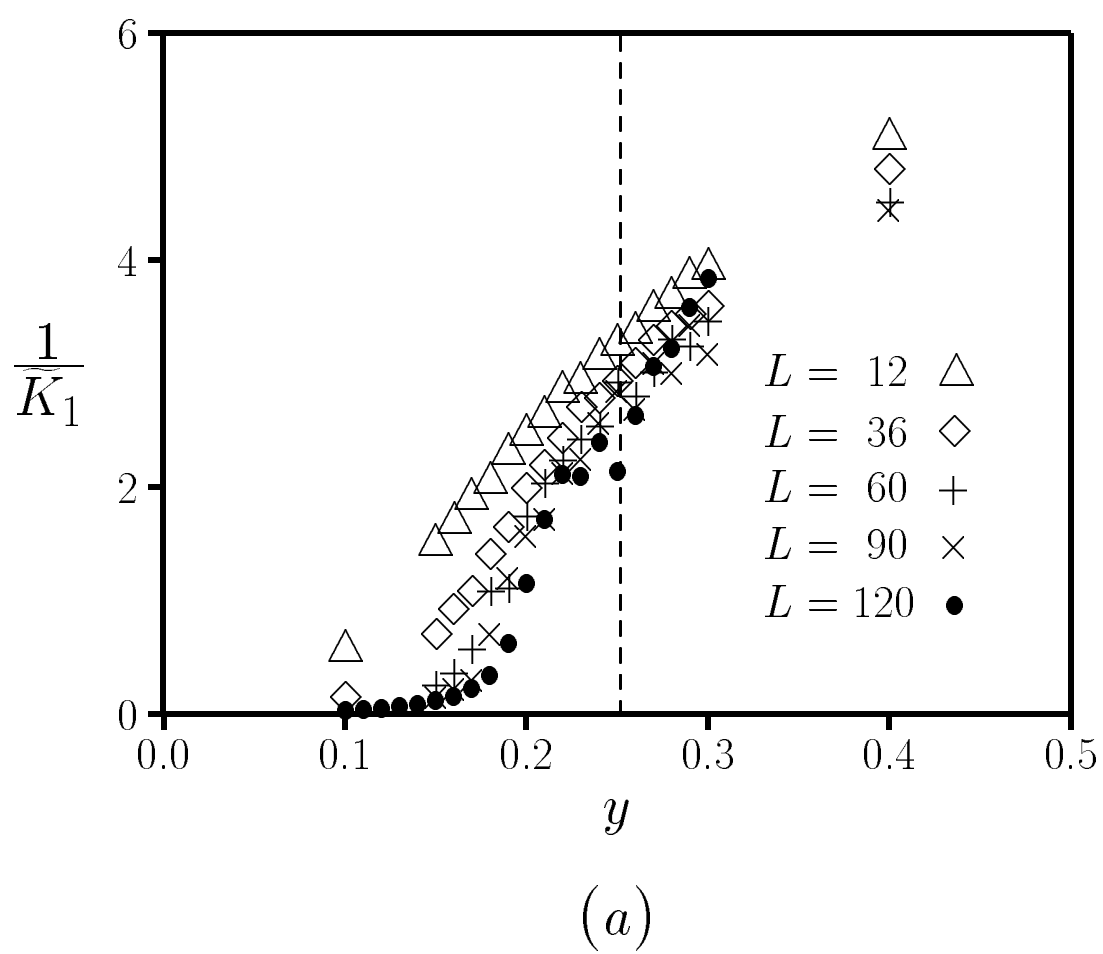


Fig. 9(a)

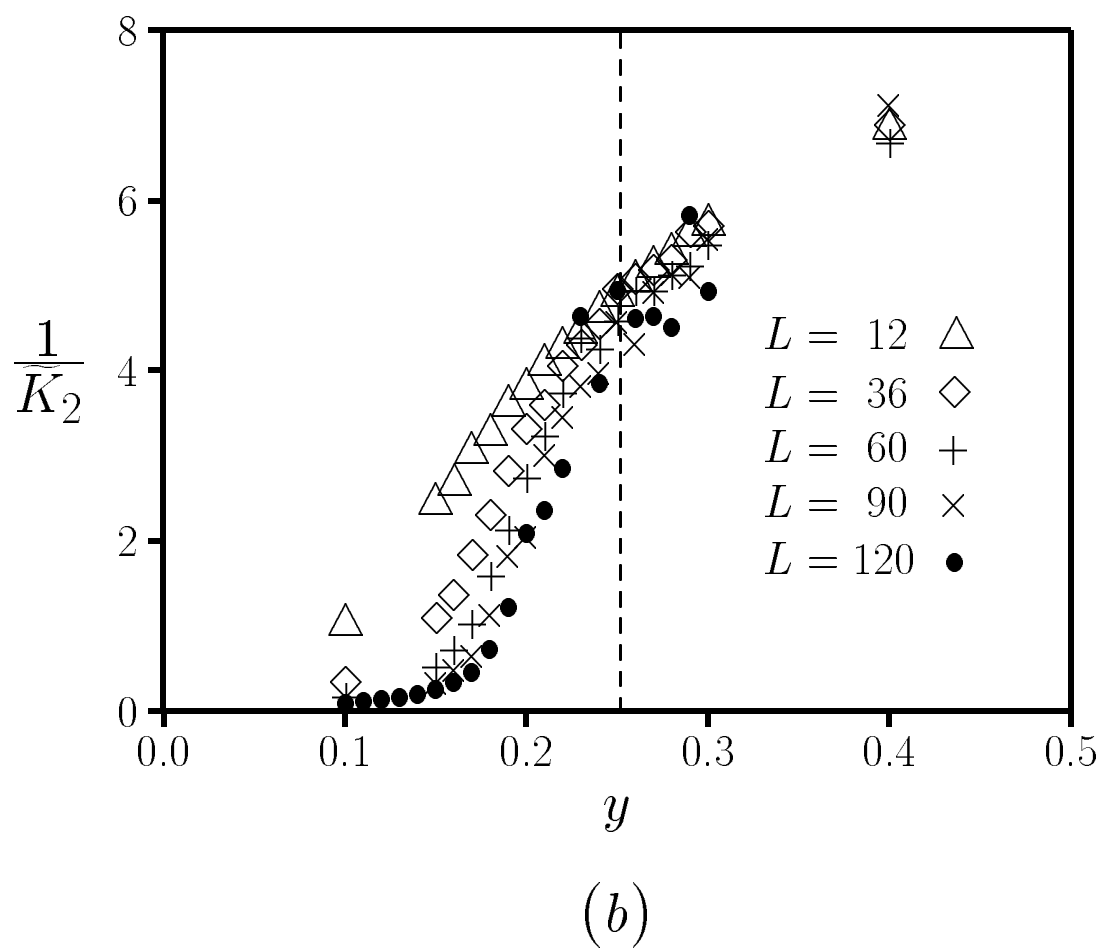


Fig. 9(b)

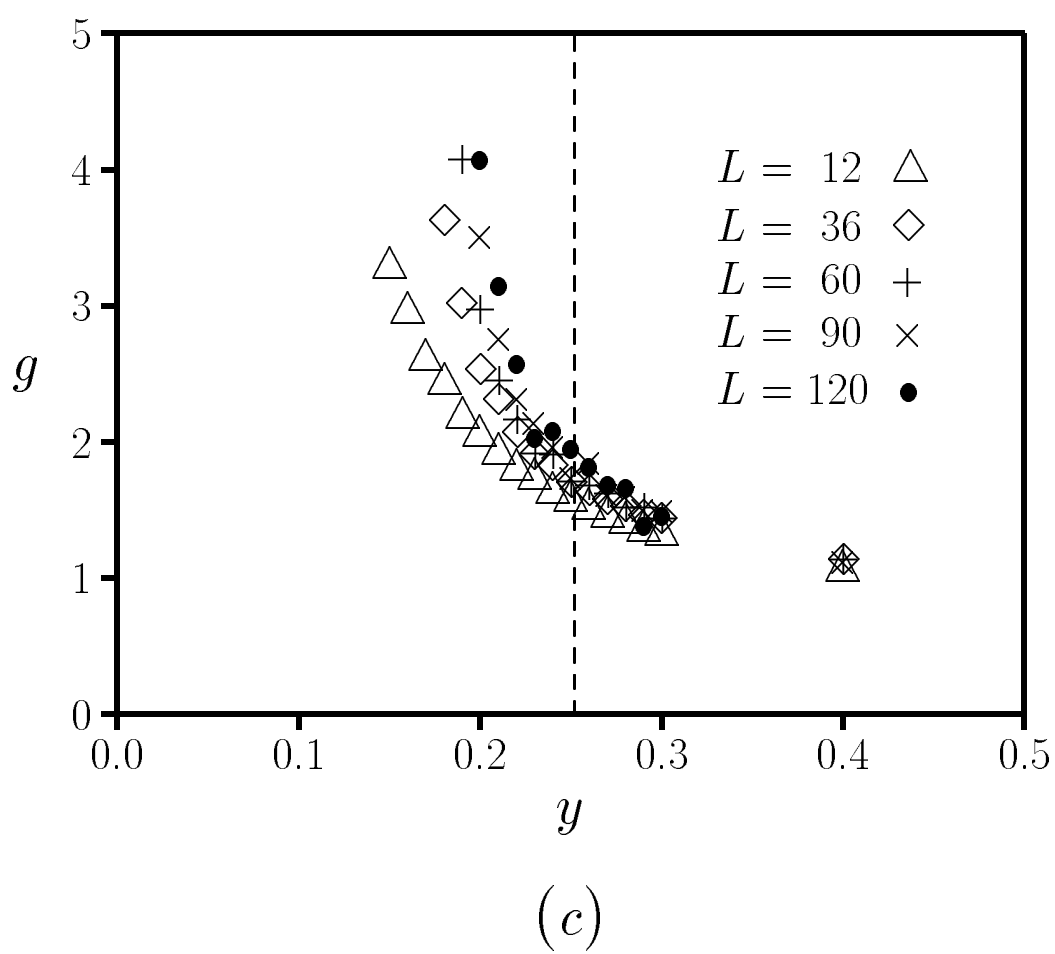


Fig. 9(c)